

DisCO: Portrait Distortion Correction with Perspective-Aware 3D GANs

Zhixiang Wang^{1,2†} Yu-Lun Liu³ Jia-Bin Huang⁴ Shin'ichi Satoh^{2,1}
Sizhuo Ma⁵ Gurunandan Krishnan⁵ Jian Wang^{5‡}

¹The University of Tokyo ²National Institute of Informatics

³National Yang Ming Chiao Tung University ⁴University of Maryland, College Park ⁵Snap Inc.

<https://portrait-disco.github.io/>



Figure 1: **Portrait distortion correction.** Portrait photos captured from a short distance (e.g., selfie) often suffer from undesired perspective distortions (the first row). Our approach corrects these perspective distortions and synthesizes visually pleasant views by *virtually* enlarging the focal length and moving the camera further away from the subject. Please check the website for videos.

Abstract

Close-up facial images captured at short distances often suffer from perspective distortion, resulting in exaggerated facial features and unnatural/unattractive appearances. We propose a simple yet effective method for correcting perspective distortions in a single close-up face. We first perform GAN inversion using a perspective-distorted input facial image by jointly optimizing the camera intrinsic/extrinsic parameters and face latent code. To address the ambiguity of joint optimization, we develop optimization scheduling, focal length reparametrization, starting from a short distance, and geometric regularization. Re-rendering the portrait at a proper focal length and camera distance effectively corrects perspective distortions and produces more natural-looking results. Our experiments show that our

method compares favorably against previous approaches qualitatively and quantitatively. We showcase numerous examples validating the applicability of our method on portrait photos in the wild. We will release our system and the evaluation protocol to facilitate future work.

1. Introduction

Every day, millions of people enjoy taking selfies with their smartphones. Although these devices have high-quality cameras that can capture high-resolution and accurate colors, selfies tend to suffer from perspective distortion. This distortion is caused by the short distance between the face and the camera (usually between 20-60 cm) and is particularly noticeable (as shown in the 1st-row of Figure 1). The distortion makes frontal features, like the nose, appear more prominent and causes the face to look unnatural and asymmetrical. Additionally, the distortion often obscures

[†]Part of the work was done while Zhixiang was an intern at Snap Research, NYC.

[‡]Corresponding author

the side of the face, including the ears. This distortion creates unflattering images and could negatively impact face identification and other related tasks.

Existing efforts automatically correct portrait perspective distortions [6, 7, 8] often involving reconstruction-based warping [17] and learning-based warping [56, 31]. However, since these methods rely on estimating a 2D flow map to warp the image, they cannot generate the disoccluded pixels, such as ears and hairs that may be revealed in the background (as shown in Figure 2(a)). The 3D photo inpainting method [41] can inpaint these disocclusion regions. However, their method is not tailored for portrait images and cannot recover faithful facial geometry such as ears (as shown in Figure 2(b)).

Our proposed solution to correct portrait perspective distortion is *3D GAN inversion*, building on the effectiveness of 3D GANs [32, 57, 10, 33, 9, 43, 15]. This approach optimizes facial latent code, camera pose, and focal length to estimate facial geometry and camera-to-face distances. However, optimizing these parameters from a single-face image is challenging, and existing GAN inversion methods like PTI [39] fail to provide accurate results when applied to 3D GANs. To address this issue, we propose three designs: (1) optimization scheduling, (2) reparameterization of focal length, and (3) initialization of camera-to-face distance to a smaller value. We also incorporate landmark and geometric constraints to improve accuracy. Our method can correct perspective distortion by adjusting the camera-to-face distance (as shown in the second row of Figure 1) and applying special visual effects such as dolly-zoom by adjusting camera parameters.

We make the following contributions:

- We propose a pipeline for correcting portrait distortion using perspective-aware 3D GAN inversion. Our pipeline differs from existing methods by generating outputs of the full-frame image, including disoccluded regions such as ears that may be revealed in new viewpoints.
- We explore several design choices to avoid the optimization falling into sub-optimal solutions, including optimization scheduling, reparameterization of the focal length to couple it with the camera-to-face distance, and better initialization.
- We establish a quantitative evaluation protocol for portrait perspective distortion correction, which will benefit future research in this area.

2. Related Work

Portrait perspective undistortion Selfie photos taken from close distances often suffer from perspective distortions, resulting in unappealing distortions such as an enlarged nose, uneven facial features, asymmetry, and hidden ears and hairs. These distortions are commonly re-

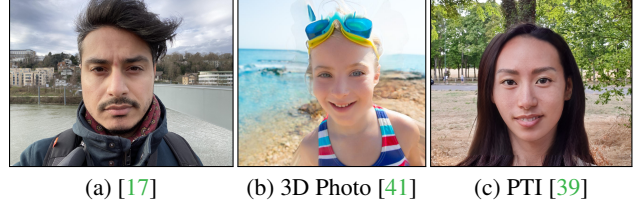


Figure 2: **Limitations of state-of-the-art portrait perspective correction techniques.** (a) [17] is a 2D warping-based method that cannot generate missing contents such as ears. (b) 3D Photo [41] is a depth-based warping method but lacks detailed face shape due to a generic depth estimator. (c) PTI [39] is a 2D GAN inversion method that may produce sub-optimal solutions and wrong facial geometry when applied to 3D GANs.

ferred to as “selfie effects” and are a significant concern for many people, with some even considering plastic surgery as a solution [51]. Research indicates that the camera distance plays a vital role in portrait perception, and studies have identified an “optimal distance” for capturing undistorted facial images [7, 12]. Specifically, it has been found that 50mm lenses are ideal for producing natural-looking and flattering images. In response, smartphone manufacturers have attempted to encourage users to take selfies from a greater distance by reducing the field of view [52].

Current perspective distortion methods either model distortion as a warping function parameter [47] or manipulate camera-to-face distance in a reconstructed model [17]. While deep learning-based methods [56] can correct minor distortions, they struggle with severe distortions due to inaccurate 3D face-fitting steps and the inability to inpaint occluded regions like ears using 2D warping flow maps. 3D radiance field-based methods [19, 4, 18] provide full control of camera parameters but require many training images and do not leverage face priors. Our method uses 3D GAN inversion to correct close-range input images, fill in unobserved regions, and allow flexible camera-to-face distances, effectively correcting severe distortions.

3D GANs The neural 3D representation [34, 29, 5, 20, 42, 35, 28, 11, 30, 48, 30] has shown impressive photorealism in novel view synthesis and serves as a foundational representation for 3D-aware generation. Implicit 3D representations have been leveraged by recently proposed 3D GANs [15, 10, 33, 57, 9, 32] to generate high-resolution outputs with remarkable details and 3D consistency. Our work uses the pre-trained architecture in EG3D [9] due to its computational efficiency and its ability to produce photorealistic 3D consistent images, similar to those generated by StyleGANs [22, 23]. However, our method is agnostic to the choice of the 3D GANs.

GAN inversion GAN inversion is a technique that maps a real image back into the latent space of a pre-trained GAN,

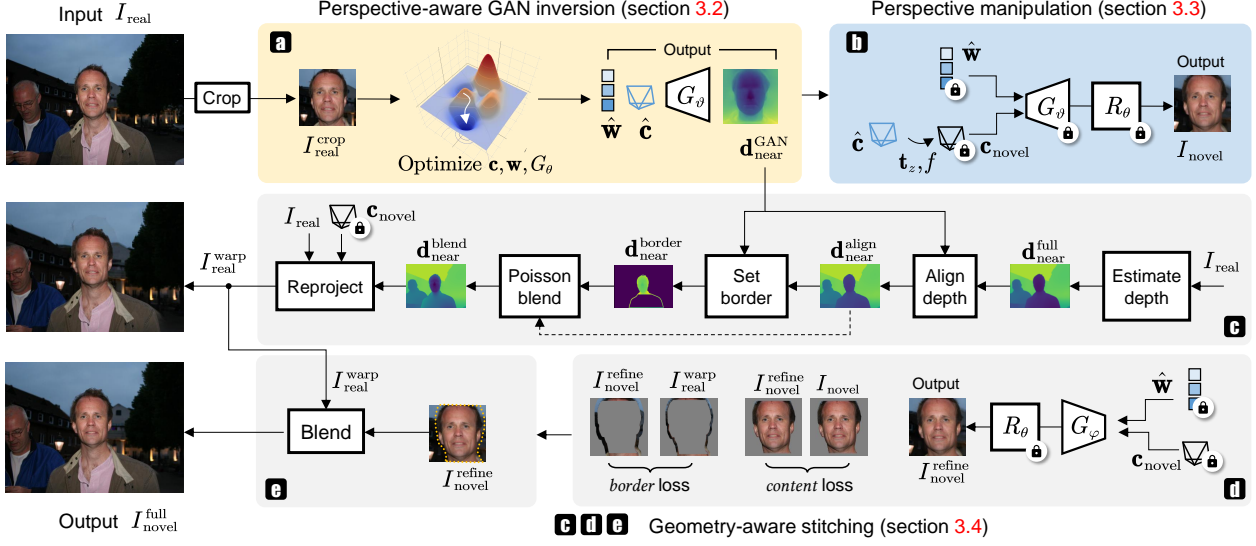


Figure 3: **Overall process of our method.** We first crop the closest face from the input image. (a) We fed the cropped face into our 3D GAN inversion to infer the face latent code and camera parameters. (b) After inversion, we manipulate the camera distance and focal length to render virtual images. (c) Then, we align and blend the GAN-rendered crop face depth map with the depth estimated from the entire image using the monocular depth estimation algorithm (MiDaS [37]). We project the entire image to the same virtual camera positions with the aligned depth. (d) To refine the border of the generated long-distance image, we fine-tune the generator by minimizing the border loss and the content loss. (e) Finally, we blend the warped full image with the generated face image.

which can expand the model’s editing capability to real photos. There are two main categories of GAN inversion: 2D and 3D. 2D GAN inversion methods optimize the latent code for a single image [1, 13] or use a learned encoder to project images to the latent space [38, 44, 3]. Some hybrid strategies combine both methods to refine the latent code by optimization [21, 58]. Recent 2D GAN inversion methods achieve high editing capabilities and have been extended for video editing [53, 45, 2]. However, editing 3D-related attributes such as camera parameters and head pose remains inconsistent and prone to severe flickering, as the pre-trained generator is unaware of the 3D structure.

3D GAN inversion methods [25, 26, 43, 49, 54] aim to achieve 3D consistent reconstruction and manipulation by jointly optimizing the face latent code and part of the camera parameters. Recent methods, such as IDE-3D [26] and Wang *et al.* [49], estimate all camera parameters from 3DMM and then keep them fixed, while Ko *et al.* [25] assume known camera intrinsics and camera-to-face distances. However, the problem is challenging due to the ambiguity among the face shape, camera-to-face distance, and focal length. To address this, we propose an optimization schedule to estimate the face latent code and camera parameters more accurately.

3. Method

Our goal is to manipulate the camera-to-subject distance of a single close-up face portrait I_{near} . To achieve this, we

propose a perspective-aware 3D GAN inversion technique that utilizes a pre-trained 3D GAN to invert the portrait into its corresponding face latent code and camera parameters. We can then adjust the camera parameters, such as the camera-to-subject distance and focal length, based on user preference. To generate a physically plausible full-frame image, we develop a workflow that warps the background and blends them together. The complete process of our technique is illustrated in Figure 3.

3.1. Preliminary

StyleGAN StyleGAN [22] maps random samples $\mathbf{z} \in \mathbb{R}^{512}$ drawn from a normal distribution to an intermediate latent vector $\mathbf{w} \in \mathbb{R}^{512}$ using a learned mapping $\mathbf{w} = H_\theta(\mathbf{z})$. The space of the latent vector \mathbf{w} (style code) is commonly referred to as W . The vector \mathbf{w} controls feature normalizations in 18 layers of the generator network G_θ and produces the final image $I = G_\theta(\mathbf{w}) = G_\theta(H_\theta(\mathbf{z}))$.

GAN inversion Inputting a real image I_{real} , we aim to seek an optimal latent vector $\hat{\mathbf{w}}$ that minimizes the similarity loss $L(\cdot)$:

$$\hat{\mathbf{w}} = \arg \min_{\mathbf{w}} L(G_\theta(\mathbf{w}), \text{Crop}((I_{\text{real}}))), \quad (1)$$

where $\text{Crop}(\cdot)$ denotes the align and crop operation that is the same as in the StyleGAN training phase. $L(\cdot)$ is usually instantiated as LPIPS [55].

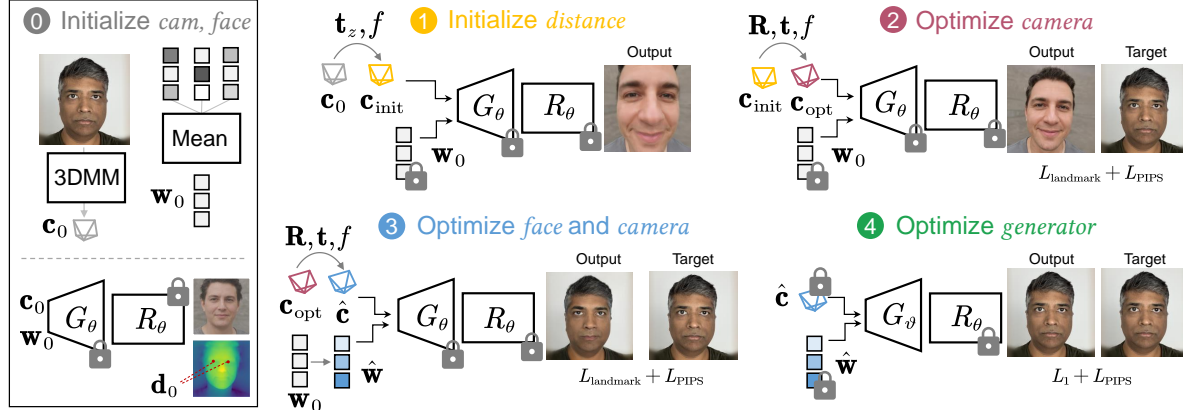


Figure 4: **Perspective-aware 3D GAN inversion.** **Step 0:** We fit a 3DMM model to the image to get an initial camera pose and average randomly sampled latent codes to initialize the face latent code. **Step 1:** We initialize the camera-to-subject distance to close ranges by adjusting the translation \mathbf{t}_z . Our focal length reparameterization relates the focal length to the distance and changes the focal length adaptively. **Step 2:** We fix the face latent code, generator, and neural renderer to optimize the camera parameters, including rotation and translation. Here, focal length also moves along with the translation \mathbf{t}_z according to our reparameterization. **Step 3:** After optimizing the camera poses, we simultaneously optimize the face latent code and camera parameters. **Step 4:** After finding optimal camera parameters and the face latent code, we fix them and fine-tune the generator to achieve high-fidelity results on real images.

3D GAN The 3D GAN model takes both latent codes and camera parameters as input to generate the final image using a neural renderer. The formulation of this process is

$$I = R_\theta(G_\theta(\mathbf{w}), \mathbf{c}) = R_\theta(G_\theta(H_\theta(\mathbf{z}, \mathbf{c})), \mathbf{c}), \quad (2)$$

where \mathbf{c} represents the intrinsic and extrinsic camera parameters and R_θ is the neural renderer. To train and invert 3D GANs, the face must also be cropped, similar to 2D GANs.

3.2. Perspective-aware 3D GAN inversion

3D GAN with additional camera parameters has shown promise in enabling camera-controllable image generation. However, it also complicates the inversion process when using a single-face image. This is because inferring unknown face and camera parameters using only appearance information is an *ill-posed* problem, which means that multiple combinations of focal lengths, camera-to-subject distances, and face shapes can generate the input image.

Existing 3D GAN inversions [43, 25] avoid this problem since they focus on face images captured at long distances, where the weak perspective model can be applied and the depth variation over the face region is negligible. The shared face shape among different combinations of focal lengths and camera-to-subject distances mitigates the ill-posedness of the problem, allowing their use of large focal lengths with roughly estimated camera-to-subject distances. Close-range photography, on the other hand, is an entirely different story. When captured at close-range distances, the ambiguity is high due to the limitation of the perspective model. Additionally, the facial appearance of the subject in the image differs from the training data [22], which assumes

long distances. These create a challenge for optimization. This is especially true when the camera estimation is inaccurate. Therefore, accurate estimation of *both* parameters is necessary to produce high-quality 3D face images.

We jointly optimize the camera-to-subject distance, the focal length, along with the latent face code:

$$\hat{\mathbf{w}}, \hat{\mathbf{c}} = \arg \min_{\mathbf{w}, \mathbf{c}} L(R_\theta(G_\theta(\mathbf{w}), \mathbf{c}), \text{Crop}(I_{\text{near}})). \quad (3)$$

To ease the ill-posedness of this optimization, we propose four key techniques: focal length reparameterization, starting from a short distance, optimization scheduling, and landmark regularization.

Focal length reparameterization Although infinitely many combinations of face shapes, focal lengths, and camera-to-subject distances exist, false combinations may result in incorrect, inverted face geometries. We propose to relate the focal length to the camera-to-subject distance to limit the degree of freedom and reduce the search space.

Suppose the world-to-camera transformation is:

$$\begin{bmatrix} p_c \\ 1 \end{bmatrix} = \begin{bmatrix} \mathbf{R} & \mathbf{T} \\ 0 & 1 \end{bmatrix} \begin{bmatrix} p_w \\ 1 \end{bmatrix}, \quad (4)$$

where $\mathbf{R} = [\mathbf{r}_x, \mathbf{r}_y, \mathbf{r}_z]^T \in \mathbb{R}^{3 \times 3}$ is the rotation matrix and $\mathbf{T} = [\mathbf{t}_x, \mathbf{t}_y, \mathbf{t}_z]^T \in \mathbb{R}^{3 \times 1}$ is the translation vector. The intrinsic matrix K transforms points from camera space to the image plane as:

$$z_c \begin{bmatrix} u \\ v \\ 1 \end{bmatrix} = K p_c = \begin{bmatrix} f & 0 & c_x \\ 0 & f & c_y \\ 0 & 0 & 1 \end{bmatrix} p_c. \quad (5)$$

Assume the initialization of translation is \mathbf{t}_{z0} , the focal length is f_0 and the camera-to-face distance is \mathbf{d}_0 . We relate the focal length f to camera translation \mathbf{t}_z by ensuring the eye position remains unchanged during the optimization. We do not optimize c_x and c_y . Besides, we do not expect the rotation changes too much. Thus, we have

$$\alpha = (\mathbf{d}_0 - (\mathbf{t}_{z0} - \mathbf{t}_z)) / \mathbf{d}_0. \quad (6)$$

We update the intrinsic matrix as

$$K = \begin{bmatrix} \gamma\alpha f_0 & 0 & c_x \\ 0 & \gamma\alpha f_0 & c_y \\ 0 & 0 & 1 \end{bmatrix}, \quad (7)$$

where γ is a learnable parameter optimized with a small learning rate to accommodate the slight error from the close-formed solution.

Starting from a short distance Besides focal length reparameterization, we also choose to start from a short camera-to-subject distance to ease optimization, as we expect to take close-up selfies as input. Specifically, we set the z -axis translation \mathbf{t}_z to a small value ϵ . At the same time, we adjust the focal length simultaneously by $f = \alpha f_0$, where α follows the close-formed solution Equation (6).

Landmark regularization The photometric loss function used in GAN inversion is ineffective for guiding perspective change. Therefore, we use a landmark loss as our additional constraint to increasing the sensibility to camera-to-subject variation. We use the dense landmarks estimated from MediaPipe [27] and calculate their L_2 distances. Since there exist many unreliable landmarks such as the occluded regions, we define an uncertainty-based landmark loss:

$$L_{\text{landmark}}(m) = \sum_{i=1}^{|\mathcal{M}|} \left(\log(\sigma_i^2) + \frac{\|m_i - m'_i\|_2^2}{2\sigma_i^2} \right), \quad (8)$$

where $m \in \mathcal{M}$ is the normalized 3D coordinates of the landmarks and $|\mathcal{M}|$ equals 468. σ is a learnable parameter to control the uncertainty.

Optimization scheduling Face and camera optimization are asynchronous. Optimization of camera-to-subject distance cannot catch up with that of face latent code. Camera parameters are prone to fall into a local minimum. Then, the face latent code will overfit the target face. Therefore, we propose a solution to schedule the optimization (see Figure 4), which sequentially optimizes the camera parameters, face latent code, and generator. We use the uncertainty-based landmark loss L_{landmark} with L_{PIPS} [55] to ensure effective camera and face optimization and minimize the L_{PIPS} with L_2 loss during generator fine-tuning to further improve image quality. Please check the appendix for our detailed algorithm.

3.3. Perspective manipulation

Upon performing 3D GAN inversion, we acquire the optimized face latent code, camera parameters, and generator. With this information, we are able to manipulate the camera distance and focal length to render virtual images I_{novel} . For instance, we can enlarge the camera-to-subject distance to correct the face perspective distortion. To ensure that the changes in focal length are appropriately aligned with the camera-to-subject distance, we utilize a closed-form solution, as defined in Equation (7).

3.4. Geometry-aware stitching

After manipulating the perspective of the face in the image, additional steps are necessary to seamlessly integrate the generated face with the rest of the image. Tzaban *et al.* [45] suggest a fine-tuning approach that focuses on minimizing the distance between the border pixels of the generated face and their corresponding pixels in the full image. By employing this strategy, their manipulated face image can be blended directly with the full image without any visible inconsistencies or artifacts.

However, our perspective manipulation with 3D GANs results in *geometric inconsistencies* between the rendered face image I_{novel} and the input image I_{real} , particularly with respect to the body and hair parts due to different distances to the camera. Directly fine-tuning the generator to composite them together would result in a distorted image with a disproportionately large face and a slim neck. To address this, we develop a method to stitch the reprojected face with the remainder of the original image, as shown in Figure 3.

Reprojection Our primary approach involves the reprojection of the entire image using the same virtual camera parameters as the rendered face to reduce geometric misalignment (Figure 3c). It requires us to have aligned depth maps for the entire image and the rendered face image. However, this process necessitates the acquisition of a depth map for the entire image aligned with the rendered face image. We first obtain the depth map $\mathbf{d}_{\text{near}}^{\text{full}}$ for the entire image using a monocular depth estimator [37], and the rendered depth map $\mathbf{d}_{\text{near}}^{\text{GAN}}$ for the cropped face using the 3D GAN method. We align these depth maps by solving

$$\arg \min_{s,b} \sum \left\| (s \times \text{Crop}(\mathbf{d}_{\text{near}}^{\text{full}} \odot \Psi) + b) - \mathbf{d}_{\text{near}}^{\text{GAN}} \right\|_2^2, \quad (9)$$

where s and b are the scale and shift, \odot is the element-wise multiplication, and Ψ is the mask of person closest to the camera. The resulting aligned depth is denoted as $\mathbf{d}_{\text{near}}^{\text{align}} = s\mathbf{d}_{\text{near}}^{\text{full}} + b$. Despite the alignment process, the aligned depth is still not perfectly aligned with the face depth due to scale and shift differences and the roughness

of the monocular depth estimator for the person. Therefore, we fuse the two depth maps by pasting the face depth $d_{\text{near}}^{\text{GAN}}$ onto the face region of $d_{\text{near}}^{\text{full}}$ and employing Poisson blending [36] to propagate the face depth to untouched body regions. The content condition $d_{\text{near}}^{\text{border}}$ is based on the rendered face depth, while the gradient follows the monocular depth. As the propagation proceeds from inner to outer regions, we add an outer boundary to $d_{\text{near}}^{\text{border}}$ using the inner border of the person’s depth map to constrain it. Following propagation, we obtain a continuous and fine-grained depth map $d_{\text{near}}^{\text{blend}}$ that aligns with the rendered face depth. Consequently, we project the entire image to a longer distance using the same camera parameters as 3D GANs.

Stitch tuning We further fine-tune the generator with the warped image to obtain the refined face image $I_{\text{novel}}^{\text{refine}}$, as depicted in Figure 3d, similar to the approach used in [46]. We use the border loss to achieve a closely-matched border between our synthesis and the warped full image:

$$L_{\text{border}} = \|I_{\text{novel}}^{\text{refine}} \odot \tilde{\Psi} - \text{CrOP}(I_{\text{real}}^{\text{warp}}) \odot \tilde{\Psi}\|_2^2, \quad (10)$$

where $\tilde{\Psi}$ is the border mask. Likewise, we maintain the integrity of the content in our synthesis via content loss:

$$L_{\text{content}} = \|I_{\text{novel}}^{\text{refine}} \odot \hat{\Psi} - I_{\text{novel}} \odot \hat{\Psi}\|_2^2, \quad (11)$$

where $\hat{\Psi}$ denotes the face inner region mask.

Composition Finally, we blend the refined synthetic face image and the warped full image to produce an entire image virtually captured at a long distance, as shown in Figure 3e.

4. Experiments

4.1. Experimental setup

Dataset (1) **Caltech Multi-Distance Portraits (CMDP) Dataset** [17]: This dataset contains portrait images of different people taken from various distances. It provides the same identities taken from different distances. We use this dataset for quantitative evaluations. (2) **USC perspective portrait database** [56]: This database contains images with single faces with different levels of perspective distortions. There are no references or ground truth images, so we only use these images for visual comparisons. (3) **In-the-wild images**: We also collect many in-the-wild photos online with severe perspective distortions on faces. We use these images for visual comparisons.

Compared methods We compare our proposed methods with two existing portrait perspective correction methods: [17] and [56], which are both 2D warping-based solutions. Since neither of them releases official implementations, we

Table 1: **Quantitative comparison on the CMDP dataset** [8]. We evaluate 43 faces projected from 60 cm to 480 cm.

Method	GAN	LMK-E↓	PSNR↑	SSIM↑	LPIPS↓	ID↑
Input	—	0.227	13.23	0.688	0.249	0.874
[17]*	✗	0.175	15.41	0.724	0.188	0.893
[17]†	✗	0.165	14.41	0.716	0.208	0.860
[39]	✓	0.191	15.92	0.717	0.197	0.758
[25]	✓	0.180	15.41	0.710	0.206	0.689
Ours	✓	0.138	17.52	0.747	0.167	0.859

*Results from their website. †Our re-implementation. Although the results differ from the original ones, the metric scores are comparable.

re-implement the method of [17]. In addition to comparing with our own implementation of the two methods, we also obtain several results from the website of [17] and the authors of [56] for comparison. Although not explicitly dealing with portrait perspective correction, 3D Photo [41] and other 2D/3D GAN inversion methods, PTI [39] and [25], are also included for comparison as they can generate novel views farther away to alleviate the perspective distortion.

Evaluation metrics We use five evaluation metrics to evaluate the performance of portrait perspective correction: (1) **Euclidean distance landmark error**: We first align all output faces, and their corresponding reference faces according to the dense facial landmarks detected via mediapipe [27]. We follow a similar alignment method by StyleGAN [22] to align the landmarks. We then calculate the normalized landmark distance error in the 2D Euclidean space. (2–4) **Photometric errors PSNR, SSIM, and LPIPS**: We also calculate photometric errors, including PSNR, SSIM [50], and LPIPS [55], between the aligned output images and corresponding references. Besides, we use a tri-map free matting algorithm [24] to remove the background and calculate the photometric distances on the masked foreground. (5) **Identity similarity**: We use ArcFace [14] to extract features for the masked face foregrounds and compute the cosine distance between facial features of output images and reference images.

4.2. Quantitative evaluation

We evaluate our proposed method on the Caltech Multi-Distance Portraits (CMDP) dataset [8]. Table 1 shows: (1) our method performs well at the landmark and photometric metrics and is equivalent to [17] in the identity metric. (2) GAN inversion-based methods [39, 25] and ours perform worse in identity preserving than warping-based methods [17]. (3) Our reimplementation of [17] is close to the original version. It performs better in the landmark metric and slightly worse in photometric metrics and the identity metric. Note that the input images are captured at about 60 cm and therefore exhibit limited perspective distortion.



Figure 5: **Qualitative comparisons on the CMDP dataset [8].** Results of [17] are from their website. Our method renders faces close to their references while preserving the identity.

4.3. Qualitative evaluation

We evaluate the proposed portrait perspective correction method on cropped face images. Figure 5 and Figure 6 show our method generates faces with fewer perspective distortions and preserves identity. Note that with the help of the 3D GAN, our method can generate occluded parts in the original input images, such as ears. We further demonstrate this advantage on faces with severe distortions and show the perspective distortion correction results in Figure 7. These visual results show that our perspective-aware 3D GAN inversion is an effective way of portrait perspective correction compared to the flow-based warping method [17] and the existing 3D GAN inversion method [25].

Besides, we validate our system’s ability to process in-the-wild full images, as demonstrated by the visually pleasing results in Figure 1 and Figure 8. Our manipulated faces show harmonious integration with corresponding bodies, with fewer distortions. In contrast, the compared methods cannot effectively reduce perspective distortion or generate harmonious results.

4.4. Ablation study

We conduct ablation studies using the entire CMDP dataset (51 faces). Since the distortion of the CMDP dataset is not severe, we also conduct the same ablation studies on our collected seriously distorted face images and show qualitative results. Figure 9 and Figure 10 show that without all our proposed designs, the optimization could easily get stuck in the sub-optimal solution and does not work well. Adding the camera optimization in the pipeline fails similarly. The proposed focal length reparameterization and the distance initialization are critical. Removing any of

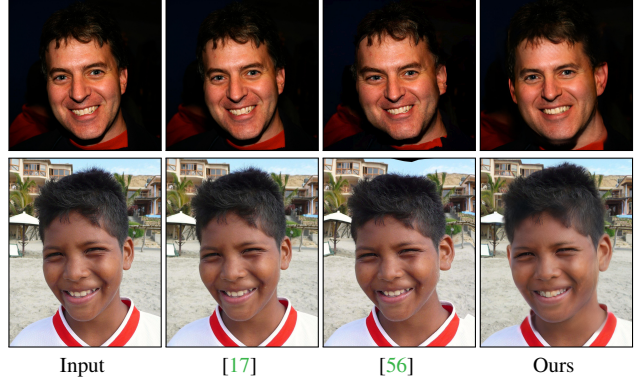


Figure 6: **Qualitative comparisons on images collected by [56].** Results of compared methods are from [56]. Our method produces the least distorted and the most natural perspective correction results. Note that with the help of 3D GAN, our method can generate the ear that originally occluded in the input images.

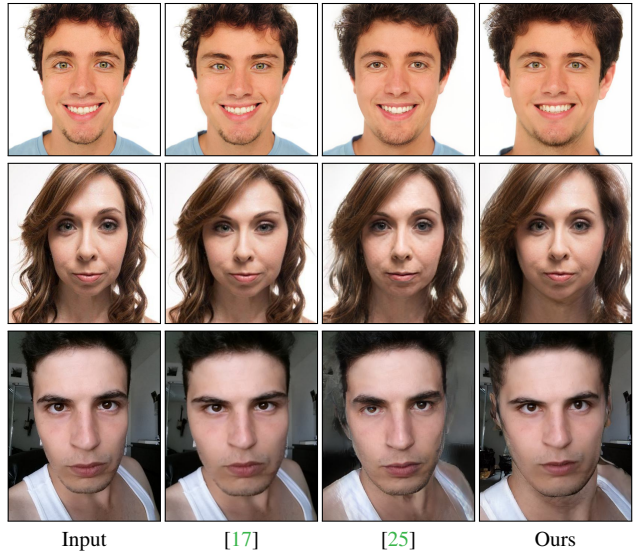


Figure 7: **Visual results for our collected severely distorted face images.** We enlarge the camera-to-subject distance to $\times 8$ times the estimated distance. Our method performs well in dealing with these seriously distorted faces and recovering occluded regions, such as ears.

them degrades the performance significantly. Optimization scheduling is also important but not the most essential.

We also conduct our pipeline’s ablation studies, including the stitching post-processing in Figure 11. Directly pasting the generated face at a distance results in an inconsistency between the face and body parts. With our further fine-tuning, we can achieve seamless blending.

4.5. Failure modes

We show some failure cases in Figure 12. Our method will fail for out-of-distribution faces, including extreme ex-



Figure 8: **Comparison on in-the-wild full images.** Results of compared methods [17, 56] are from [56]. Our system produces a visually pleasing result with the least distortions. Note that our rendered face is harmonious with the body.

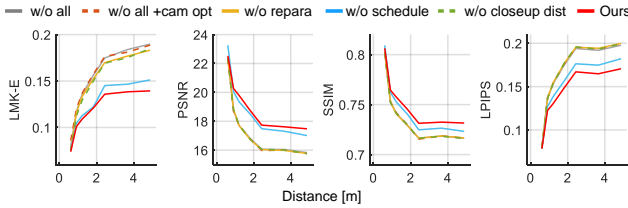


Figure 9: **Quantitative results of ablation study.** (1) 3D GAN inversion w/o all of our designs does not work. (2) 3D GAN inversion with camera optimization (cam opt) performs similarly to w/o all. (3) Focal length reparameterization and distance initialization are crucial. Removing any of them (w/o repara and w/o close-up dist) significantly degrades performance. (4) Without optimization scheduling (w/o schedule) also degrades the performance. (5) Our method achieves the best performance.

pressions, occluded faces (by hand or other objects), and faces with high-frequency details like moles, freckles, ornament, tattoos, *etc.*, due to the limited training set of the pre-trained GAN. For the first two cases, GAN inversion cannot understand the face and may generate the face in its own understanding (see the left example of Figure 12 where the tongue is interpreted as part of the lip in the output), which sometimes has awful artifacts (see the right example of Figure 12 where hand looks bad in the output). For the third case, GAN inversion may ignore the high-frequency details and output a smoothed-out face.

5. Conclusions

We present a method for portrait perspective distortion correction. Our core idea is to leverage a 3D GAN inversion method to recover plausible facial geometry and reveal hidden facial parts such as ears. We explore several design choices such as optimization scheduling, focal length reparameterization, closeup camera-to-face distance initial-

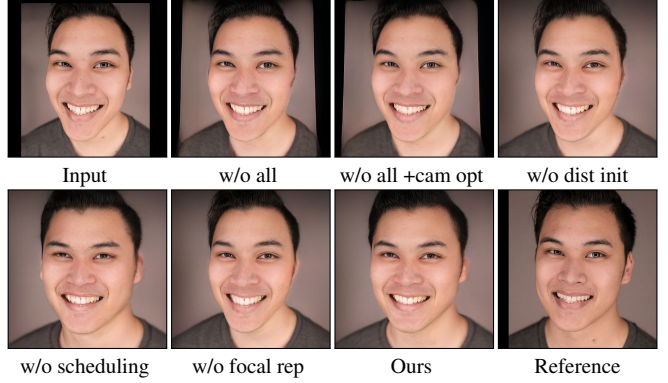


Figure 10: **Qualitative results of ablation study.** Our full model produces a visually pleasing result close to the reference. We found that 3D GAN inversion without our designs or with camera optimization incorporated could not correct perspective distortion effectively. Our approach still performs well without some key designs, such as camera-to-subject distance initialization and focal length reparameterization. Although optimization scheduling is not dominant in our method, it is necessary to avoid sub-optimal results due to ambiguity between face, camera-to-subject distance, and focal length.

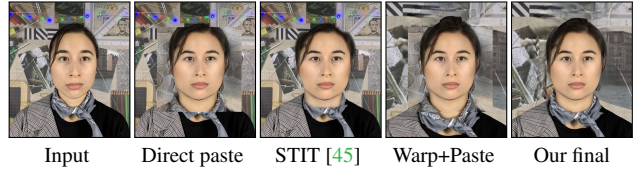


Figure 11: **Qualitative results for ablation study of our pipeline.** Our 3D GAN inversion can reproject a cropped face image to a virtual far distance, but the untouched regions of the image can become distorted. If we simply paste the modified face back into the original image, the result may have a geometry inconsistency between the cropped face and the untouched regions. Even applying the method outlined in [45] to the “direct paste” approach may not work. This geometry inconsistency is alleviated after warping the background. Whereas the seam between cropped regions and the original image is still apparent. We further tune the generator to achieve seamless blending.



Figure 12: **Failure cases.** Limited by the training set of GAN, our method cannot handle out-of-distribution faces, *e.g.*, tongue outside the mouth, hand touch face. A partial solution is to first mask these regions for GAN inversion. Then, transfer the textures to the manipulated face.

ization, and landmark constraints. Furthermore, we establish a protocol of quantitative evaluation for the portrait

perspective distortion correction. Quantitative and visual comparisons demonstrate the improved performance of our pipeline over existing methods.

References

- [1] Rameen Abdal, Yipeng Qin, and Peter Wonka. Image2stylegan: How to embed images into the stylegan latent space? In *ICCV*, 2019. 3
- [2] Rameen Abdal, Peihao Zhu, Niloy J Mitra, and Peter Wonka. Video2stylegan: Disentangling local and global variations in a video. *arXiv preprint arXiv:2205.13996*, 2022. 3
- [3] Yuval Alaluf, Or Patashnik, and Daniel Cohen-Or. Restyle: A residual-based stylegan encoder via iterative refinement. In *ICCV*, 2021. 3
- [4] ShahRukh Athar, Zexiang Xu, Kalyan Sunkavalli, Eli Shechtman, and Zhixin Shu. Rignervf: Fully controllable neural 3d portraits. In *CVPR*, 2022. 2
- [5] Matan Atzmon and Yaron Lipman. SAL: Sign agnostic learning of shapes from raw data. In *CVPR*, 2020. 2
- [6] Thabo Beeler, Bernd Bickel, Paul Beardsley, Bob Sumner, and Markus Gross. High-quality single-shot capture of facial geometry. In *ACM TOG (Proc. SIGGRAPH)*. 2010. 2
- [7] Ronnie Bryan, Pietro Perona, and Ralph Adolphs. Perspective distortion from interpersonal distance is an implicit visual cue for social judgments of faces. 2012. 2
- [8] Xavier P Burgos-Artizzu, Matteo Ruggero Ronchi, and Pietro Perona. Distance estimation of an unknown person from a portrait. In *ECCV*, 2014. 2, 6, 7
- [9] Eric R Chan, Connor Z Lin, Matthew A Chan, Koki Nagano, Boxiao Pan, Shalini De Mello, Orazio Gallo, Leonidas J Guibas, Jonathan Tremblay, Sameh Khamis, et al. Efficient geometry-aware 3d generative adversarial networks. In *CVPR*, 2022. 2, 11
- [10] Eric R Chan, Marco Monteiro, Petr Kellnhofer, Jiajun Wu, and Gordon Wetzstein. pi-GAN: Periodic implicit generative adversarial networks for 3D-aware image synthesis. In *CVPR*, 2021. 2
- [11] Zhiqin Chen and Hao Zhang. Learning implicit fields for generative shape modeling. In *CVPR*, 2019. 2
- [12] Emily A Cooper, Elise A Piazza, and Martin S Banks. The perceptual basis of common photographic practice. *Journal of vision*, 2012. 2
- [13] Antonia Creswell and Anil Anthony Bharath. Inverting the generator of a generative adversarial network. *IEEE transactions on neural networks and learning systems*, 2018. 3
- [14] Jiankang Deng, Jia Guo, Niannan Xue, and Stefanos Zafeiriou. Arcface: Additive angular margin loss for deep face recognition. In *CVPR*, 2019. 6
- [15] Yu Deng, Jiaolong Yang, Jianfeng Xiang, and Xin Tong. Gram: Generative radiance manifolds for 3D-aware image generation. In *CVPR*, 2022. 2
- [16] Yu Deng, Jiaolong Yang, Sicheng Xu, Dong Chen, Yunde Jia, and Xin Tong. Accurate 3d face reconstruction with weakly-supervised learning: From single image to image set. In *CVPRW*, 2019. 11
- [17] Ohad Fried, Eli Shechtman, Dan B Goldman, and Adam Finkelstein. Perspective-aware manipulation of portrait photos. *ACM TOG (Proc. SIGGRAPH)*, 2016. 2, 6, 7, 8
- [18] Guy Gafni, Justus Thies, Michael Zollhofer, and Matthias Nießner. Dynamic neural radiance fields for monocular 4d facial avatar reconstruction. In *CVPR*, 2021. 2
- [19] Chen Gao, Yichang Shih, Wei-Sheng Lai, Chia-Kai Liang, and Jia-Bin Huang. Portrait neural radiance fields from a single image. *arXiv preprint arXiv:2012.05903*, 2020. 2
- [20] Amos Gropp, Lior Yariv, Niv Haim, Matan Atzmon, and Yaron Lipman. Implicit geometric regularization for learning shapes. In *Proc. ICML*, 2020. 2
- [21] Shanyan Guan, Ying Tai, Bingbing Ni, Feida Zhu, Feiyue Huang, and Xiaokang Yang. Collaborative learning for faster stylegan embedding. *arXiv preprint arXiv:2007.01758*, 2020. 3
- [22] Tero Karras, Samuli Laine, and Timo Aila. A style-based generator architecture for generative adversarial networks. In *CVPR*, 2019. 2, 3, 4, 6, 11
- [23] Tero Karras, Samuli Laine, Miika Aittala, Janne Hellsten, Jaakko Lehtinen, and Timo Aila. Analyzing and improving the image quality of stylegan. In *CVPR*, 2020. 2
- [24] Zhanghan Ke, Jiayu Sun, Kaican Li, Qiong Yan, and Rynson W.H. Lau. Modnet: Real-time trimap-free portrait matting via objective decomposition. In *AAAI*, 2022. 6, 11
- [25] Jaehoon Ko, Kyusun Cho, Daewon Choi, Kwangrok Ryoo, and Seungryong Kim. 3d gan inversion with pose optimization. In *Proceedings of the IEEE/CVF Winter Conference on Applications of Computer Vision*, 2023. 3, 4, 6, 7, 8
- [26] Connor Z Lin, David B Lindell, Eric R Chan, and Gordon Wetzstein. 3d gan inversion for controllable portrait image animation. *arXiv preprint arXiv:2203.13441*, 2022. 3
- [27] Camillo Lugaresi, Jiuqiang Tang, Hadon Nash, Chris McClanahan, Esha Uboweja, Michael Hays, Fan Zhang, Chuoling Chang, Ming Guang Yong, Juhyun Lee, et al. Mediapipe: A framework for building perception pipelines. *arXiv preprint arXiv:1906.08172*, 2019. 5, 6
- [28] Lars Mescheder, Michael Oechsle, Michael Niemeyer, Sebastian Nowozin, and Andreas Geiger. Occupancy networks: Learning 3d reconstruction in function space. In *CVPR*, 2019. 2
- [29] Mateusz Michalkiewicz, Jhony K Pontes, Dominic Jack, Mahsa Baktashmotlagh, and Anders Eriksson. Implicit surface representations as layers in neural networks. In *Proc. ICCV*, 2019. 2
- [30] Ben Mildenhall, Pratul P Srinivasan, Matthew Tancik, Jonathan T Barron, Ravi Ramamoorthi, and Ren Ng. Nerf: Representing scenes as neural radiance fields for view synthesis. In *ECCV*, 2020. 2
- [31] Koki Nagano, Huiwen Luo, Zejian Wang, Jaewoo Seo, Jun Xing, Liwen Hu, Lingyu Wei, and Hao Li. Deep face normalization. *ACM TOG (Proc. SIGGRAPH)*, 38(6):1–16, 2019. 2
- [32] Michael Niemeyer and Andreas Geiger. Giraffe: Representing scenes as compositional generative neural feature fields. In *CVPR*, 2021. 2

- [33] Roy Or-El, Xuan Luo, Mengyi Shan, Eli Shechtman, Jeong Joon Park, and Ira Kemelmacher-Shlizerman. Stylesdf: High-resolution 3D-consistent image and geometry generation. In *CVPR*, 2022. 2
- [34] Jeong Joon Park, Peter Florence, Julian Straub, Richard Newcombe, and Steven Lovegrove. DeepSDF: Learning continuous signed distance functions for shape representation. In *CVPR*, 2019. 2
- [35] Songyou Peng, Michael Niemeyer, Lars Mescheder, Marc Pollefeys, and Andreas Geiger. Convolutional occupancy networks. In *ECCV*, 2020. 2
- [36] Patrick Pérez, Michel Gangnet, and Andrew Blake. Poisson image editing. In *SIGGRAPH*, 2003. 6
- [37] René Ranftl, Katrin Lasinger, David Hafner, Konrad Schindler, and Vladlen Koltun. Towards robust monocular depth estimation: Mixing datasets for zero-shot cross-dataset transfer. *IEEE TPAMI*, 2020. 3, 5, 11
- [38] Elad Richardson, Yuval Alaluf, Or Patashnik, Yotam Nitzan, Yaniv Azar, Stav Shapiro, and Daniel Cohen-Or. Encoding in style: a stylegan encoder for image-to-image translation. In *CVPR*, 2021. 3
- [39] Daniel Roich, Ron Mokady, Amit H Bermano, and Daniel Cohen-Or. Pivotal tuning for latent-based editing of real images. *ACM TOG (Proc. SIGGRAPH)*, 2021. 2, 6
- [40] Robin Rombach, Andreas Blattmann, Dominik Lorenz, Patrick Esser, and Björn Ommer. High-resolution image synthesis with latent diffusion models, 2021. 11
- [41] Meng-Li Shih, Shih-Yang Su, Johannes Kopf, and Jia-Bin Huang. 3d photography using context-aware layered depth inpainting. In *CVPR*, 2020. 2, 6, 8, 11
- [42] Vincent Sitzmann, Michael Zollhöfer, and Gordon Wetzstein. Scene representation networks: Continuous 3d-structure-aware neural scene representations. In *Proc. NeurIPS 2019*, 2019. 2
- [43] Jingxiang Sun, Xuan Wang, Yichun Shi, Lizhen Wang, Jue Wang, and Yebin Liu. Ide-3d: Interactive disentangled editing for high-resolution 3d-aware portrait synthesis. *arXiv preprint arXiv:2205.15517*, 2022. 2, 3, 4, 11
- [44] Omer Tov, Yuval Alaluf, Yotam Nitzan, Or Patashnik, and Daniel Cohen-Or. Designing an encoder for stylegan image manipulation. *ACM TOG (Proc. SIGGRAPH)*, 2021. 3
- [45] Rotem Tzaban, Ron Mokady, Rinon Gal, Amit Bermano, and Daniel Cohen-Or. Stitch it in time: GAN-based facial editing of real videos. In *SIGGRAPH Asia*, 2022. 3, 5, 8
- [46] Rotem Tzaban, Ron Mokady, Rinon Gal, Amit Bermano, and Daniel Cohen-Or. Stitch it in time: Gan-based facial editing of real videos. In *ACM TOG (Proc. SIGGRAPH Asia)*, 2022. 6
- [47] Joachim Valente and Stefano Soatto. Perspective distortion modeling, learning and compensation. In *CVPRW*, 2015. 2
- [48] Peng Wang, Lingjie Liu, Yuan Liu, Christian Theobalt, Taku Komura, and Wenping Wang. Neus: Learning neural implicit surfaces by volume rendering for multi-view reconstruction. *arXiv preprint arXiv:2106.10689*, 2021. 2
- [49] Youjia Wang, Teng Xu, Yiwen Wu, Minzhang Li, Wenzheng Chen, Lan Xu, and Jingyi Yu. Narrate: A normal assisted free-view portrait stylizer. *arXiv preprint arXiv:2207.00974*, 2022. 3
- [50] Zhou Wang, Alan C Bovik, Hamid R Sheikh, and Eero P Simoncelli. Image quality assessment: from error visibility to structural similarity. *IEEE TIP*, 2004. 6
- [51] Brittany Ward, Max Ward, Ohad Fried, and Boris Paskhover. Nasal distortion in short-distance photographs: the selfie effect. *JAMA facial plastic surgery*, 2018. 2
- [52] Kenta K Williams and Ricardo Motta. Camera field of view effects based on device orientation and scene content, July 18 2017. US Patent 9,712,751. 2
- [53] Yiran Xu, Badour AlBahar, and Jia-Bin Huang. Temporally consistent semantic video editing. In *ECCV*, 2022. 3
- [54] Yiran Xu, Zhixin Shu, Cameron Smith, Jia-Bin Huang, and Seoung Wug Oh. In-n-out: Face video inversion and editing with volumetric decomposition. *arXiv preprint arXiv:2302.04871*, 2023. 3
- [55] Richard Zhang, Phillip Isola, Alexei A Efros, Eli Shechtman, and Oliver Wang. The unreasonable effectiveness of deep features as a perceptual metric. In *CVPR*, 2018. 3, 5, 6, 11
- [56] Yajie Zhao, Zeng Huang, Tianye Li, Weikai Chen, Chloe LeGendre, Xinglei Ren, Ari Shapiro, and Hao Li. Learning perspective undistortion of portraits. In *ICCV*, 2019. 2, 6, 7, 8
- [57] Peng Zhou, Lingxi Xie, Bingbing Ni, and Qi Tian. Cips-3d: A 3D-aware generator of GANs based on conditionally-independent pixel synthesis. *arXiv preprint arXiv:2110.09788*, 2021. 2
- [58] Jun-Yan Zhu, Philipp Krähenbühl, Eli Shechtman, and Alexei A Efros. Generative visual manipulation on the natural image manifold. In *ECCV*, 2016. 3

A. Implementation Details

A.1. The Proposed Workflow

In our experiments, we employ the EG3D model [9] pre-trained on the FFHQ dataset [22]. Our method, however, is agnostic to the underlining 3D GAN models. For example, other 3D GANs such as IDE-3D [43] could also be used. We initialize the camera parameters by fitting a 3DMM [16], consistent with the EG3D training process, ensuring the compatibility between the initialized camera parameters and EG3D. For monocular depth estimation, we incorporate the MiDaS approach [37]. Additionally, we employ 3D Photo Inpainting [41] to reproject the background, including partial body and hair elements.

As 3D Photo Inpainting [41] may not sufficiently reveal the hidden background and could result in undesirable gaps, we first use Stable Diffusion [40] or DALL·E2 to inpaint the background when processing full-frame input images. We then reproject the inpainted background and utilize it for replacing the background in our rendered full-frame image. For this task, we leverage MODNet [24] to separate the person from the background.

A.2. Perspective-aware 3D GAN Inversion

Algorithm 1 presents our proposed perspective-aware 3D GAN inversion. We initialize the camera parameters \mathbf{c}_0 by fitting a 3DMM and the face latent code by averaging random sample vectors: $\mathbf{w}_0 = 1/N \sum_{i=1}^N H_\theta(\mathbf{z}_i)$. This initialization allows the 3D GAN to render a depth map, with the eye depth \mathbf{d}_0 ensuring a consistent inter-pupil distance. Subsequently, we optimize the camera parameters, face latent code, and generator sequentially. Upon completing optimization, we obtain the inverted face latent code, camera parameters, optimized generator, and other relevant parameters, enabling us to perform perspective manipulation.

A.3. Rotation Reparameterization

Besides focal length parameterization, we also reparametrize the rotation matrix \mathbf{R} to ensure orthogonality and reduce the degree of freedom:

$$\mathbf{R} = \begin{bmatrix} | & | & | \\ \mathbf{r}_x & \mathbf{r}_y & \mathbf{r}_z \\ | & | & | \end{bmatrix} = F(\mathbf{Q}) = F\left(\begin{bmatrix} | & | \\ \mathbf{q}_1 & \mathbf{q}_2 \\ | & | \end{bmatrix}\right), \quad (12)$$

where $\mathbf{r}_x, \mathbf{r}_y, \mathbf{r}_z \in \mathbb{R}^3$ are $\mathbf{r}_x = N(\mathbf{q}_1)$, $\mathbf{r}_y = N(\mathbf{q}_2 - (\mathbf{r}_x \cdot \mathbf{q}_2)\mathbf{r}_x)$, and $\mathbf{r}_z = \mathbf{r}_x \times \mathbf{r}_y$, and $N(\cdot)$ denotes L_2 norm. We directly replace \mathbf{R} with \mathbf{Q} in Algorithm 1.

A.4. Losses

a) During camera and face optimization, we minimize a combination of uncertainty-based landmark loss and LPIPS [55]: $L = L_{\text{PIPS}} + L_{\text{landmark}}$. b) To further enhance

Algorithm 1: Optimization procedure

Input: Pre-trained generator G_θ , initialized face latent code \mathbf{w}_0 and camera parameter \mathbf{c}_0 with focal length f_0 and z -axis translation \mathbf{t}_{z0} , and the camera-to-face distance \mathbf{d}_0 .
Output: Optimized camera parameter $\hat{\mathbf{c}}$, face latent code $\hat{\mathbf{w}}$, generator $G_{\hat{\theta}}$, and updated parameters \mathbf{d}_0 , f_0 and \mathbf{t}_{z0} .

```

1 // Initialization
2 Initialize  $\mathbf{c} \leftarrow \mathbf{c}_0$ ,  $\mathbf{w} \leftarrow \mathbf{w}_0$ ,  $\mathbf{t} \leftarrow \epsilon$ ,  $\delta \mathbf{t}_z \leftarrow 1$ ,  $\gamma \leftarrow 1$ .
3 Get  $\alpha$  according to Equation (6).
4 Update  $f \leftarrow \alpha f_0$ .

5 // Optimize camera parameters
6 Fix face latent code  $\mathbf{w}$ , weights of  $G_\theta$ .
7 while iterations  $k < 300$  do
8   Get the gradients  $\nabla_{\mathbf{t}}, \nabla_{\mathbf{R}}, \nabla_{\gamma}$ .
9   Optimize  $\delta \mathbf{t}_z \leftarrow \delta \mathbf{t}_z + \lambda_{\text{cam}} \nabla_{\mathbf{t}}$ .
10  Optimize  $\mathbf{t}_z \leftarrow \mathbf{t}_{z0} / \sqrt{\delta \mathbf{t}_z}$ .
11  Get  $\alpha$  according to Equation (6).
12  Update  $f \leftarrow \gamma \alpha f_0$ .
13  Optimize  $\mathbf{p} \leftarrow \mathbf{p} + \lambda_{\text{tiny}} \times \lambda_{\text{cam}} \nabla_{\mathbf{p}}$ ,  $\mathbf{p} \in \{\mathbf{R}, \mathbf{t}_x, \mathbf{t}_y, \gamma\}$ .
14 end

15 // Optimize camera and face parameters
16 Fix weights of  $G_\theta$ .
17 while iterations  $k < 700$  do
18   Get the gradients  $\nabla_{\mathbf{t}}, \nabla_{\mathbf{R}}, \nabla_{\mathbf{w}}, \nabla_{\gamma}$ .
19   Optimize  $\delta \mathbf{t}_z \leftarrow \delta \mathbf{t}_z + \lambda_{\text{cam}} \nabla_{\mathbf{t}}$ .
20   Optimize  $\mathbf{t}_z \leftarrow \mathbf{t}_{z0} / \sqrt{\delta \mathbf{t}_z}$ .
21   Optimize  $\mathbf{w} \leftarrow \mathbf{w} + \lambda_{\text{face}} \nabla_{\mathbf{w}}$ .
22   Get  $\alpha$  according to Equation (6).
23   Update  $f \leftarrow \gamma \alpha f_0$ .
24   Optimize  $\mathbf{p} \leftarrow \mathbf{p} + \lambda_{\text{tiny}} \times \lambda_{\text{cam}} \nabla_{\mathbf{p}}$ ,  $\mathbf{p} \in \{\mathbf{R}, \mathbf{t}_x, \mathbf{t}_y, \gamma\}$ .
25 end

26 // Optimize generator
27 Fix face latent code  $\mathbf{w}$ , camera parameters  $\mathbf{c}$ .
28 while not converge do
29   Get the gradients  $\nabla_{\theta}$ .
30   Optimize  $G_{\hat{\theta}} \leftarrow G_\theta + \lambda_{\text{gan}} \nabla_{\theta}$ .
31 end
32 Update  $\hat{\mathbf{c}} \leftarrow \mathbf{c}$ ,  $\hat{\mathbf{w}} \leftarrow \mathbf{w}$ 
33 Get  $\mathbf{d}$ 
34 Update  $\mathbf{d}_0 \leftarrow \mathbf{d}$ ,  $f_0 \leftarrow f$ ,  $\mathbf{t}_{z0} \leftarrow \mathbf{t}_z$ 

```

image quality, we minimize the combination of LPIPS loss and L_2 during generator fine-tuning: $L = L_{\text{PIPS}} + L_2$. Additionally, in both a) and b), we apply masks to the black borders. c) We optimize the combination of border loss and content loss during geometry-aware stitching tuning: $L = L_{\text{border}} + L_{\text{content}}$.

A.5. Parameters Setting

We set learning rates λ_{face} to 1×10^{-2} , λ_{face} to 5×10^{-3} , λ_{gan} to 3×10^{-4} , and λ_{tiny} to 0.1. We let the parameter ϵ equal 0.5. We set the rendering parameters `ray_start` and `ray_end` to `auto` for close-up faces.